19th Brazilian Congress of Thermal Sciences and Engineering
November 06th-10th, 2022, Bento Gonçalves - RS - Brazil

ENC-2022-0546
HIGH-SPEED IMAGING OF FLOW BOILING IN ASYMMETRIC DUAL-V MICROCHANNELS WITH TAPERED MANIFOLD

Debora C. Moreira*
Jorge Nicolau dos Santos
Valter S. do Nascimento Junior
Heat Transfer Research Group (HTRG), Department of Mechanical Engineering, São Carlos School of Engineering – University of São Paulo (EESC/USP)
*dcmoreira@usp.br
Satish G. Kandlikar
Thermal Analysis, Microfluidics and Fuel Cells Laboratory (TAμFL), Mechanical Engineering Department, Rochester Institute of Technology (RIT)
Gherhardt Ribatski
Heat Transfer Research Group (HTRG), Department of Mechanical Engineering, São Carlos School of Engineering – University of São Paulo (EESC/USP)

Abstract. *Flow boiling in microchannels is a promising thermal management solution for high heat flux dissipation from restricted spaces. High heat transfer capability at relatively low temperature gradients provided by the exchange of latent heat together with the low volume of fluid required in microchannel-based systems are some of the most desirable characteristics in such applications. However, to date the foreseen performance of flow boiling heat transfer in microchannel-based heat sinks is yet to be achieved, mainly due to significant instabilities that resulted in prohibitive pressure drop, early critical heat flux, and lower than expected heat transfer coefficient. In general, the reported instabilities are closely related to the confined growth of bubbles, fluid maldistribution and interaction between channels, and some techniques were proposed to improve the overall performance of these heat sinks. Recently, encouraging results were obtained during flow boiling of water over microstructured surfaces containing asymmetric Dual-V microchannels with an open and tapered manifold. The performance was attributed to the successful combination of previously employed strategies to enhance pool and flow boiling heat transfer, promoting bubble cross-flow and inducing separate liquid and vapor pathways. The main goal of this work is to assess bubble movement through high-speed images, identifying possible preferential directions and quantifying their velocities. The high-speed images were obtained during flow boiling experiments conducted with deionized water at four distinct flow rates varying from 60 – 340 ml/min for a heat flux dissipation that reached 580 W/cm^2. An acquisition rate of 18000 fps at a resolution of 128 x 256 was selected for images of single bubbles. The movement of bubbles was tracked through interface and pattern identification algorithms using Matlab, revealing the bubble cross-flow caused by the microstructured surface. Further investigation will be conducted combining imaging analysis with heat transfer performances so it can be verified if the performance improvement can be attributed to the movement of bubbles.*

Keywords: *Bubble tracking, Pattern recognition, Cross-flow, Heat transfer enhancement.*

1. INTRODUCTION

The demand for high heat flux cooling technologies has motivated a great interest in flow boiling heat transfer in microchannels-based heat sinks over the last decades (Benam et al., 2021). The possibility of removing major heat loads from restricted spaces with reduced temperature gradients and using working fluids with adequate saturation temperatures to the expected applications are some desirable characteristics of this technology, which for a fixed pumping power can dissipate more heat than single-phase liquid flows (Ribatski et al., 2007). It is well known that bubble dynamics and the resultant flow patterns have significant effects on the heat transfer performance of evaporators, and this influence is accounted in numerous heat transfer prediction methods (Cheng and Xia, 2017), like the one proposed by Costa-Patry and Thome (2013) and the one proposed by Kuznetsov et al. (2013).

Despite the evident importance of this subject for a thorough comprehension of flow boiling phenomena and for the development of highly efficient microchannels-based heat sinks (Wu and Sundén, 2014), experimental investigation on

bubble dynamics based on high-speed images are relatively scarce, and often the applied methodologies in such studies are not well documented to be successfully reproduced. Bogojevic et al. (2013) analyzed the water bubble growth characteristics in heat sinks containing parallel rectangular microchannels during subcooled and saturated flow boiling. Varying bubble diameters were measured using the ImageJ software and images acquired at 1000 fps with a resolution of 1280 x 1024 pixels by a high-speed camera mounted on a microscope with a 5x magnification objective, and their results have evidenced three stages of bubbles growth and a significant influence of bubble dynamics in the observed temperature and pressure fluctuations. Kalani and Kandlikar (2015a) acquired top images at 3000 to 10000 fps of the flow patterns along the entire heat sinks with open and tapered manifold of water flow boiling on a plain surface and parallel microchannels, so they observed bubbles nucleating at the base of the channels and growing on the fin top until detaching into the open manifold and merging with other bubbles. This behavior was indicated by them as the main enhancement mechanism for the observed improvement in heat transfer performance promoted by their heat sink configuration. Prajapati et al. (2017) investigated the growth rate of water bubbles inside three distinct configurations of micro heat sinks based on images acquired by a high-speed camera at 1000 fps, and concluded that fluctuations in pressure and temperature measurements reduced with the heat sink configuration with segmented channels that enabled lateral growth of bubbles. Recently, Parahovnik and Peles (2022) conducted flow boiling experiments with near-critical carbon dioxide and evaluated the diameter and velocities of bubbles, as well as the interaction between bubbles using high speed-images from a camera mounted on a microscope with a 10x magnification lens, and reported good agreement of the thermally-driven model with experimental velocity results for single bubbles, while strong deviations were observed after bubbles started interacting.

According to the literature regarding bubble dynamics in microchannels, it can be observed that the identification of dominating heat transfer mechanisms is strongly dependent on bubble dynamics, and it is still not clear how the mechanisms are affected in each regime of bubble growth and the influence of the bubble paths, which are rarely reported (Kadam et al., 2021). A recent design of heat sink proposed by Moreira et al. (2022) strongly relies on the expected patterns of bubble movements; hence, the main goal of this work is to present a methodology to identify and track bubble paths, in order to verify if the bubbles that nucleate on the microstructured surface proposed in our previous work effectively detach in cross-flow trajectories. This methodology can be further expanded to automatically provide the size and velocities of bubbles, and to identify the positions of active nucleation sites, if the heat sink can be successfully illuminated by a diffuse light source, reducing reflection and shadowing effects.

2. MATERIALS AND EXPERIMENTAL METHODS

The experimental campaign from this work is part of a broad investigation performed by Moreira et al. (2022), such that the configuration of the test section, experimental apparatus and test conditions are briefly described in this section, while further details can be found in our previous work (Moreira et. al, 2022). The test section used in this work consisted of a copper chip with microstructured surface designed to interact with nucleating bubbles and direct them in a certain way to create preferential liquid and vapor paths, similarly to what was proposed by Kandlikar (2013) for pool boiling. Thus, the concept of the employed surface was based on pairs of asymmetric V-shaped microchannels, called Dual-V grooves, which were machined in copper chips along the 10 mm flow length. The expected trajectory of nucleating bubbles is shown schematically for an asymmetric Dual V-groove with one side normal to the base as seen in Fig. 1, reprinted from (Moreira et al., 2022). Heat was applied to the flow through the 10 mm x 10 mm footprint area, and a polysulfone cover with the open and tapered manifold enabled flow visualization from the top of the test section. Images from experiments conducted with a sample containing five Dual-V channels 400 μm high above the reference surface with V internal angles equal to 60° were used in this work, since the movement of single bubbles was better observed in wider channels.

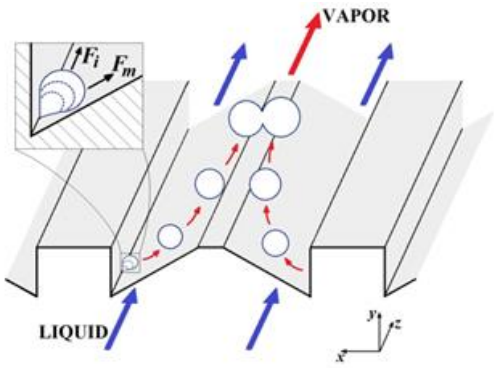

Figure 1. Expected trajectory of nucleating bubbles in the Dual-V groove microchannels. Reprinted from (Moreira et al., 2022)

Flow boiling experiments were conducted with distilled water in the same setup as the one used by Kalani and Kandlikar (2015a,b). The copper chips were combined with a tapered manifold fabricated in polysulfone that defined the flow area and enabled flow visualization. An aluminum spacer was employed to fix the minimum gap height, while a silicone gasket was responsible for sealing the assembled test section. The employed taper was 6%, meaning that the gap height above the channels top increased by 600 μm, from 127 to 727 μm along the length of 10 mm, which was the best performing manifold configuration selected by Kalani and Kandlikar (2015b). The top flow images were acquired with a Photron 1024 Fastcam CMOS high-speed camera and a 150 mm Nikon lens, set at 18000 fps and 1/20000 s-1 shutter speed, with resolutions of 256 x 128. A Dolan-Jenner Fiber-lite MH-100 metal halide Machine Vision Illuminator lamp was used as light source.

3. IMAGE PROCESSING METHOD

The image processing methodology employed in this work consisted on identifying the nucleation growth and detachment process of single bubbles, such that their movement could be tracked, and the influence of the microstructured surface on this behavior was properly assessed. The bubble tracking algorithm consists in four main steps: image pre-processing, location of boundary contours and definition of dominant points, fitting ellipses to the located contours, and tracing bubble paths. The first step to apply this algorithm was to select short footages acquired at 18000 fps in which the processes of nucleation, growth and detachment of singular bubbles were identified, the frames in which the whole process of singular bubbles were observed were manually selected and named. Then, for a sequence of three frames of monochromatic images $\boldsymbol{A}$, $\boldsymbol{B}$ and $\boldsymbol{C}$ defined as:

$$\boldsymbol{A},\boldsymbol{B},\boldsymbol{C} = \left\{p_{ij}\middle| i = 1,2,\dots,M; j = 1,2,\dots,N; 0 \le p_{i,j} \le 2^b - 1\right\}, \tag{1}$$

where M and N are the image dimensions, $p_{i,j}$ is the intensity value associated to the pixel with coordinates (i,j), and b is the image bit depth. The first operation that was conducted is the stretching of intensity values in each image $\boldsymbol{I}$ using the function F_{adjust}, so the minimum $p_{i,j}$ value becomes 0 and the maximum $p_{i,j}$ value turns into 1:

$$F_{adjust}(\boldsymbol{I}) = \left\{\frac{p_{ij} - \min \boldsymbol{I}}{\max \boldsymbol{I} - \min \boldsymbol{I}}\middle| i = 1,2,\dots,M; j = 1,2,\dots,N\right\}. \tag{2}$$

Then, the screen blend of two successive images $\boldsymbol{A}(p_{i,j})$ and $\boldsymbol{B}(q_{i,j})$ with the same resolution $M \times N$ was performed through the function F_{screen}, producing enlightened images:

$$F_{screen}(\boldsymbol{A},\boldsymbol{B}) = \left\{1 - \left(1 - p_{i,j}\right) \times \left(1 - q_{i,j}\right)\middle| i = 1,2,\dots,M; j = 1,2,\dots,N\right\} \tag{3}$$

And the difference of two successive screen blends $\boldsymbol{S_1}=F_{screen}(\boldsymbol{A},\boldsymbol{B})$ and $\boldsymbol{S_2}=F_{screen}(\boldsymbol{B},\boldsymbol{C})$ was employed to eliminate the background:

$$F_{difference}(\boldsymbol{S_1},\boldsymbol{S_2}) = \left\{\left|p_{i,j} - q_{i,j}\right|\middle| i = 1,2,\dots,M; j = 1,2,\dots,N\right\}. \tag{4}$$

After background exclusion, the remaining noise was removed by applying the function $F_{db4filter}$, which is a filter function based on the four level wavelet transform using the Daubechies wavelet with four vanishing moments and a threshold of 0.2 in each level, so a binarization process was conducted in the noise-free image for a selected binarization level of 0.15:

$$F_{binarize}(\boldsymbol{I}) = \left\{1 \text{ if } p_{i,j} \ge 0.15; \text{ else } 0\middle| i = 1,2,\dots,M; j = 1,2,\dots,N\right\} \tag{5}$$

Due to the non-uniform illumination, the resultant binarized images presented separated chunks of the bubbles that corresponded to the reflectance of the curved interfaces. Thus, the morphological closing operation F_{close} was performed, which consisted of sequential dilation and erosion processes of the image with a structuring element of a 6 pixels radius disk for both operations. Finally, objects that were smaller than 30 pixels after the closing process were removed from the image with the function $F_{areaopen}$, reducing false detection. The pre-processing procedure is illustrated in Fig. 2, with the resulting contours of two identified elements that correspond to the bubble of interest and to a portion of another interface from a vapor slug, together with its dominant points.

For all objects in the final pre-processed image, the contours of the objects were tracked and stored by a contour-tracing algorithm in clockwise direction with four connecting neighborhoods, creating for each object a sequence of coordinate points. Then, the number of points related to each object contour was significantly reduced using the method for identification of dominant points presented by Zhang et al. (2012), which for a sequence of N coordinate points that describe the whole contour $\boldsymbol{c}$,

$$\boldsymbol{c} = \{p_i(x_i, y_i) | i = 1,2, \dots, N\} \quad (6)$$

with p_i being the i[th] point of the contour with coordinates (x_i,y_i) and neighbors p_{i-1} and p_{i+1}, extracts a set of dominant points $\boldsymbol{c}_{dom}$ that are representative of that contour, based on the criterion of the minimum perpendicular distance Dcrit from a midpoint of a segment to the chord defined by the extremities of that segment, representing a local curvature estimation based on a polygonal approximation. The perpendicular distance of a point p_j to the chord $\overline{p_i p_k}$ is

$$D_{j,\overline{ik}} = \sqrt{\frac{(x_k - x_j)(y_i - y_j) - (y_k - y_j)(x_i - x_j)}{(x_j - x_i)^2 + (y_j - y_i)^2}}, \quad (7)$$

given that $i < j < k$; $i, j, k \in \mathbb{Z}$ and

$$j = \left\lfloor \frac{i+k}{2} \right\rfloor \quad (8)$$

D_{crit} was set to 0.5 in this work, which is the same value adopted by Zhang et al. (2012). Then, the main algorithm for the detection of dominant points by local curvature estimation, based on a polygonal approximation, proceeds as follows:

m = FLOOR(N/2) % m is the max size of search region
S_{new} = {$p_{new,i} = p_i$, i = 1,2,. . . ,N} U { $p_{new,i} = p_{i-N}$, , i = N+1,N+2,. . . ,N+m}
i ← 1
WHILE i ≤ N
  FOR k = 2 to m
    $p_I \leftarrow p_{new,i}$; $p_K \leftarrow p_{new,k}$; $p_J \leftarrow p_{new,i+floor((k-1)/2)}$
    IF $D_{j,ik} \geq D_{crit} \cap i+k > N+m$
      BREAK;
    ENDIF
  ENDFOR
  $p_{new.k}$ is a dominant point
  i ← i + k;
ENDWHILE

After the identification of dominant points, marked in yellow in the last image of Fig. 2, ellipses were fitted to the identified objects using a stable direct least square fitting method described by Halir and Flusser (1998) to estimate the ellipse parameters, which was implemented in the function $F_{ellipsefit}$, and for each sequence of *N* dominant points associated to an object in the image $\boldsymbol{c}_{dom}$, the ellipse radii, center position and axis inclination were returned.

FOR EACH $\boldsymbol{c}_{dom}$
  $Ellipse_{new} = F_{ellipseFitting}(\boldsymbol{c}_{dom})$
ENDFOR

After the ellipses of each object were determined in the current frame, the algorithm recognized if the bubbles were present in the previous frame, tracing the bubble's trajectory based on the varying position of the center of the bubble. Hence, the center of each ellipse identified in one frame was compared to the center of each ellipse from the previous frame, and if the distance of the center positions of bubbles in two sequential frames was shorter than five pixels, the routine recognized it as the same bubble that moved and traced its path, with the implemented algorithm:

FOR EACH $Ellipse_i$ IN current frame
  FOR EACH $Ellipse_j$ IN previous frame
    $Distance_{ij}$ is the centers distance of $Ellipse_i$ centered on (cx_i, cy_i) and $Ellipse_j$ centered on (cx_j, cy_j)
    IF $Distance_{ij}$ is the minimal distance U $Distance_{ij} \leq$ maximum acceptable distance
    THEN i and j is the same bubble and the path is from (cx_j, cy_j) to (cx_i, cy_i)
  ENDFOR
ENDFOR

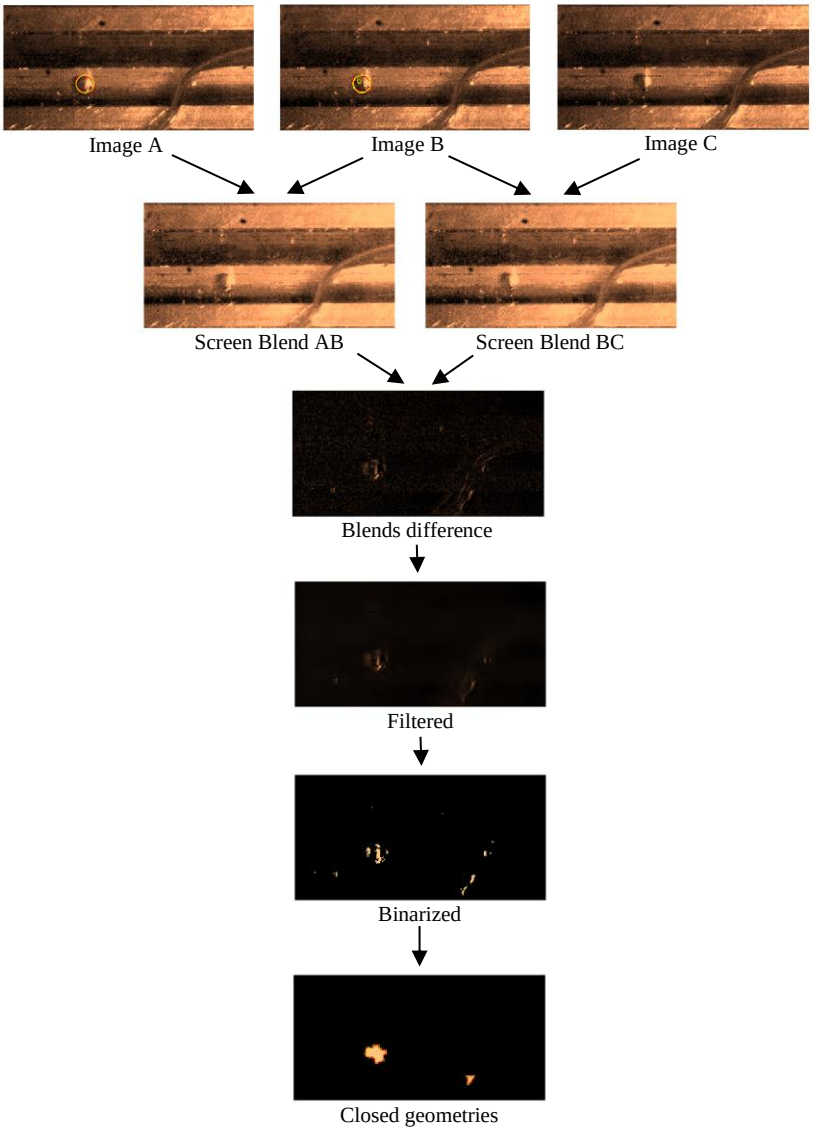

Figure 2. Image pre-processing for the application of the FitEllipse algorithm.

Figure 3 shows the identified ellipses and traced trajectories superimposed in one frame. It should be noted that due to the non-uniformity of the illumination during the experiments, some regions of the images were saturated, while others became too dark, and resulted in the identification of false bubbles by the algorithm and the apparent vanishing of the bubble of interest. This was solved with manual selection and exclusion of false bubbles, as well as integrating separated trajectories of the bubble of interest, but the current algorithm can be further improved to automatically join separate paths of the bubble of interest by evaluating the distances from the bubbles identified in more frames than just the previous one, and other parameters could be optimized to reduce false detection. Another aspect that should be remarked is that the employed routine to fit ellipses is able to identify the centers and radii, but at this point these measurements were not considered, because they are strongly influenced by the conducted morphologic operations. In contrast, the position of bubble center and the traced trajectory were verified against the images, showing good accuracy. An interesting feature worth noting in Fig. 3 is that the bubble of interest first slides over the surface while pinned to the bottom of the channel until it suddenly detaches from the vertical wall in the direction of the inclined surface, exactly in the way the microstructures were designed to interact with the generated bubbles.

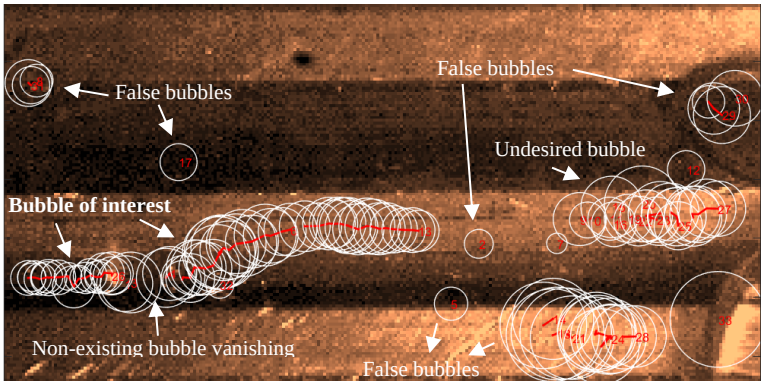

Figure 3. Traced trajectories based on a sequence of images.

4. RESULTS AND DISCUSSION

Preliminary results for bubble tracking are presented and discussed in this section. The obtained results show that we can successfully track bubble paths, which can be further processed to quantify the displacements and velocity of bubbles, although some drawbacks related to the experimental arrangement and image acquisition and treatment parameters could be identified, showing directions to further improve the proposed methodology. As described by Moreira et al. (2022), the proposed surfaces were designed such that the bubbles could nucleate along the inner corners of the Dual-V channels and detached in a traverse direction, creating preferential vapor paths on top of the inclined surfaces, while liquid paths could flow over the rectangular fins. This expected traverse movement of a single bubble can be seen in the sequence of high-speed images shown in Fig. 4. The vertical side of one V-channel is highlighted by an orange line in the images, while the bubble evidenced by a blue line is seen to nucleate at 0 ms and grows at the corner while still pinned to the vertical wall. From 1 ms onwards, the bubble is seen to move away from the vertical wall in a cross-flow direction, and flow over the inclined wall of the V-channel until eventually emerging into the open microgap region and collapsing (not shown in these frames), since this footage corresponds to a subcooled flow.

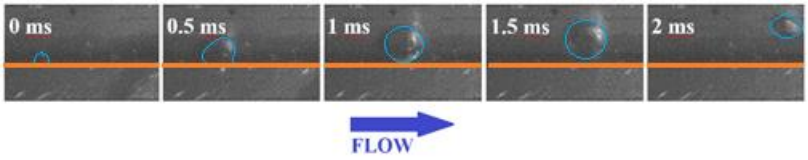

Figure 4. High-speed images acquired at 18,000 fps (top) and diagrams (bottom) of bubble cross-flow in sample #2, with 60º Dual-V channels at 60 ml/min and 180 W/cm^2. Time intervals between the images are 0.5 ms.

The bubble movement seen in Fig. 4 indicates that the vertical wall effectively drives the bubble towards the inclined surface due to the effects of the evaporation momentum force. Similar footages to the one presented in Fig. 4 containing five distinct bubbles identified in the full sequence of high-speed images taken at 18,000 fps during flow boiling experiment at 60 ml/min and 180 W/cm^2 were selected and analyzed with the methodology presented in section 3, so the trajectories of these bubbles were tracked and the time evolution of the distance of their center to the vertical wall with an uncertainty of ±40 μm is plotted in Fig. 5.

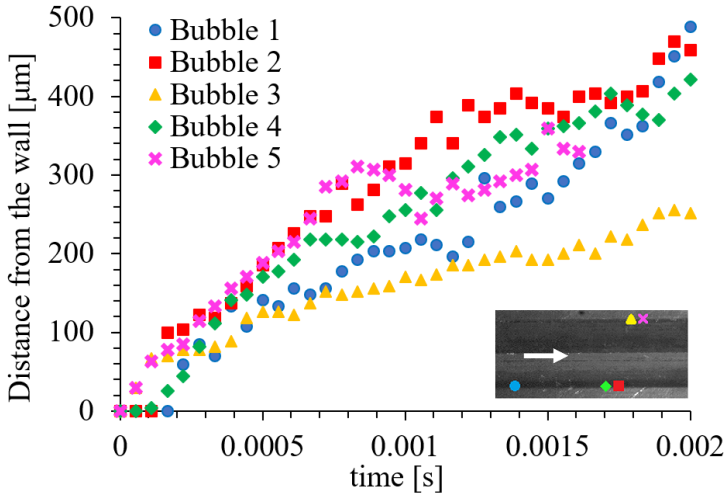

Figure 5. Distances from bubbles center to the vertical wall at five nucleation sites. The inset shows the top view of a 5 mm long portion of the channels with indicated positions of nucleation sites for each bubble that was tracked. The white arrow indicates flow direction reprinted from (Moreira et al., 2022).

Results displayed in Fig. 5 clearly show that the behavior observed in Fig. 4 occur at distinct nucleation sites, independent of their position, and that the methodology proposed in this work was successful in identifying and tracking bubbles. The variation that is observed with time happens because of interactions with the main flow, which are more intense as the bubbles grow, and especially after detachment.

5. CONCLUSIONS

This paper presented a methodology to identify and trace bubbles trajectories based on high-speed images of flow boiling experiments. This approach was applied to images acquired during water flow boiling experiments using a recently proposed design of heat sink based on Dual-V groove microchannels combined with a tapered manifold, and preliminary results show that the microstructured surface effectively drives the bubbles away from vertical walls and towards the inclination, which causes a separation of preferential liquid and vapor streams. It was identified that lateral expansion of vapor bubbles and coalescence of bubbles coming from distinct Dual-V groves hinder the formation of separate liquid-vapor paths. Further improvement of our methodology includes the definition of ideal acquisition frequency to quantify the displacements and velocities, reduction in false detection and bubble vanishing, and the automatic measurement of the diameter of single bubbles.

6. ACKNOWLEDGEMENTS

The authors would like to acknowledge the financial support provided by FAPESP through the grants #2015/24834-3, #2016/09509-1, #2017/12576-5, and #2018/23538-0. The technical support provided by Rick Wurzer and Craig Arnold from the ME Department at RIT in the fabrication of the microstructured copper chips and manifolds is also recognized and deeply appreciated.

7. REFERENCES

Benam, B. P., Sadaghiani, A. K., Yağcı, V., Parlak, M., Sefiane, K., and Koşar, A., 2021. Review on high heat flux flow boiling of refrigerants and water for electronics cooling. *International Journal of Heat and Mass Transfer*, Vol. 180, pp. 121787.

Bogojevic, D., Sefiane, K., Duursma, G., nd Walton, A. J., 2013. Bubble dynamics and flow boiling instabilities in microchannels. *International Journal of Heat and Mass Transfer*, Vol. 58(1-2), pp. 663-675.

Cheng, L., and Xia, G., 2017. Fundamental issues, mechanisms and models of flow boiling heat transfer in microscale channels. *International Journal of Heat and Mass Transfer,* Vol. 108, pp. 97-127.

Costa-Patry, E., and Thome, J. R., 2013. Flow pattern-based flow boiling heat transfer model for microchannels. *International Journal of Refrigeration*, Vol. 36(2), pp. 414-420.

Halir, R. and Flusser. J., 1998. Numerically stable direct least squares fitting of ellipses. In: *Proceedings of the 6th International Conference in Central Europe on Computer Graphics and Visualization*, WSCG, Plzen, Czech Republic, pp. 125–132.

Kadam, S. T., Hassan, I., Kumar, R., and Rahman, M. A., 2021. Bubble dynamics in microchannel: An overview of the state-of-the-art. *Meccanica*, Vol. 56(3), pp. 481-513.

Kalani, A., and Kandlikar, S. G., 2015a. Flow patterns and heat transfer mechanisms during flow boiling over open microchannels in tapered manifold (OMM). *International Journal of Heat and Mass Transfer*, Vol. 89, pp. 494-504.

Kalani, A. and Kandlikar, S.G., 2015b. Effect of taper on pressure recovery during flow boiling in open microchannels with manifold using homogeneous flow model. *International Journal of Heat and Mass Transfer*, Vol. 83, pp. 109-117.

Kandlikar, S.G., 2013. Controlling bubble motion over heated surface through evaporation momentum force to enhance pool boiling heat transfer. *Applied Physics Letters*, Vol. 102(5), pp. 051611.

Kuznetsov, V. V., Shamirzaev, A. S., Kozulin, I. A., and Kozlov, S. P., 2013. Correlation of the flow pattern and flow boiling heat transfer in microchannels. Heat transfer engineering, Vol. 34(2-3), pp. 235-245.

Moreira, D.C., Nascimento, V.S., Ribatski, G., and Kandlikar, S.G., 2022. Combining liquid inertia and evaporation momentum forces to achieve flow boiling inversion and performance enhancement in asymmetric Dual V-groove microchannels. *International Journal of Heat and Mass Transfer*, Vol. 194, pp. 123009.

Parahovnik, A., and Peles, Y., 2022. Bubble dynamics in a subcooled flow boiling of near-critical carbon dioxide. *International Journal of Heat and Mass Transfer*, Vol. 183, pp. 122191.

Prajapati, Y. K., Pathak, M., and Khan, M. K., 2017. Bubble dynamics and flow boiling characteristics in three different microchannel configurations. *International Journal of Thermal Sciences*, Vol. 112, pp. 371-382.

Ribatski, G., Cabezas-Gómez, L., Navarro, H. A., & Saíz-Jabardo, J. M., 2007. The advantages of evaporation in micro-scale channels to cool microeletronic devices. *Revista de Engenharia Térmica*, Vol. 6(2), pp. 34-39.

Wu, Z., and Sunden, B., 2014. On further enhancement of single-phase and flow boiling heat transfer in micro/minichannels. *Renewable and Sustainable Energy Reviews*, Vol. 40, pp. 11-27.

Zhang, W., Jiang, X. and Liu, Y., 2012. A method for recognizing overlapping elliptical bubbles in bubble image. *Pattern Recognition Letters*, Vol. 33, pp. 1543-1548.

8. RESPONSIBILITY NOTICE

The authors are the only responsible for the printed material included in this paper.